Theoretical Study of the Catalytic Hydrogenation of Alkenes by a Disilaferracyclic Complex: Can the Fe−Si σ-Bond-Assisted Activation of H−H Bonds Allow Development of a Catalysis of Iron?

Atsushi Tahara,[†] Hiromasa Tanaka,[†] Yusuke Sunada,[†] Yoshihito Shiota,[†] Kazunari Yoshizawa,[†] and Hideo Nagashima*,[†,‡,§]

[†]Institute for Materials Chemistry and Engineering and [‡]Graduate School of Engineering Sciences, Kyushu University, Kasugakoen 6-1, Kasuga-shi, Fukuoka, Japan

[§]CREST, Japan Science and Technology Agency, Tokyo 102-0076, Japan

S *Supporting Information*

ABSTRACT: The mechanisms associated with the hydrogenation of alkenes catalyzed by the iron complex Fe(*cis*-CO)$_2${*o*-(SiMe$_2$)$_2$C$_6$H$_4$}$_2$(H)$_2$ (**1**) were investigated by DFT calculations. The complex **1** has a structure in which the iron center is bonded to four silicon atoms and two hydrides. Secondary Si···H···Si interactions were also observed. The exchange of a 1,2-bis(dimethylsilyl)benzene ligand with ethylene and hydrogen gives a disilaferracycle bearing η^2-(CH$_2$=CH$_2$) and η^2-H$_2$ ligands. The catalytic cycle initiated from the disilaferracycle involves cleavage of a H−H linkage assisted by an Fe−Si bond to form Fe−H and η^1-(H−Si) moieties (step 1), hydrogen migration from the Fe−H group to the η^2-(CH$_2$=CH$_2$) ligand which accomplishes the insertion of ethylene into the Fe−H bond (step 2), and reaction of the resulting β-agostic ethyl moiety with the η^2-(H−Si) group to form ethane on the iron atom (step 3). The octahedral geometry of **1** as well as the presence of π-acidic CO ligands and Fe−Si σ-bonds contributes to all of the catalytic intermediates and the transition states being in the low-spin state. Steps 1 and 3 correspond to the σ-complex-assisted metathesis (σ-CAM) mechanisms proposed by Perutz and Sabo-Etienne, suggesting that these mechanisms can assist in the design of iron-based hydrogenation catalysts operating under mild conditions.

Fe-Si σ-Bond-assisted Activation of a H-H Bond
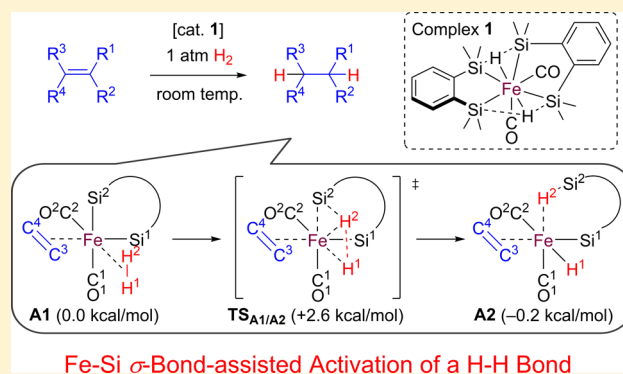
INTRODUCTION

The catalytic hydrogenation of unsaturated molecules by transition metal complexes is one of the most fundamental reactions in homogeneous catalysis.[1] Various catalysts based on noble metal complexes, in particular, rhodium and ruthenium phosphine complexes, have been developed. These allow useful synthetic protocols to produce a wide variety of organic molecules, typically via the reduction of ketones and/or hydrogenation of alkenes.[1b] Conventionally, catalytic cycles involving the oxidative addition of a coordinated H$_2$ molecule to a reactive center have been employed for the hydrogenation of both ketones and alkenes. Typical examples are shown in Scheme 1a; the oxidative addition of H$_2$ to the metal (M) forms a H−M−H species, and this step is followed by the insertion of a C=C or C=O bond into one of the M−H bonds. Reductive elimination of the product proceeds from the resulting hydride−alkyl or hydride−alkoxy metal species.[1c]

A new approach to the hydrogenation of ketones, the so-called "metal−ligand cooperation" concept, has been proposed by Noyori and co-workers, as shown in Scheme 1b.[2] Several ruthenium(II) complexes bearing 2,2′-bis(diphenylphosphino)-

1,1′-binaphthyl (BINAP) and bidentate diamine ligands have been found to efficiently catalyze the hydrogenation of ketones, in conjunction with high enantioselectivity. In this process, the heterolytic cleavage of the coordinated η^2-H$_2$ ligand by the action of an electronegative nitrogen atom bonded to the ruthenium center produces both Ru−H(δ−) and N−H(δ+) moieties, which contribute to the efficient reduction of polar C=O bonds in the outersphere of the metal. This method has since been widely adopted for the development of new catalysts for the hydrogenation of carbonyl compounds.

One unique approach to understanding the hydrogenation of alkenes via metal−ligand cooperation is the σ-complex-assisted metathesis (σ-CAM) mechanism proposed by Sabo-Etienne and Perutz in 2007.[3] This process involves cleavage of the H−H bond of a η^2-H$_2$ ligand, assisted by a metal−E bond (E = carbon, boron, silicon). Scheme 1c shows a proposed mechanism for this catalytic cycle, in which σ-bond metathesis of the M−E bond of an E−M−alkyl species based on late

Scheme 1. Catalytic Cycles for Hydrogenation of Unsaturated Molecules Involving (a) Conventional Oxidative Addition of H$_2$ to the Metal, (b) Metal−Ligand Cooperation for H−H Heterolytic Cleavage, and (c) σ-CAM-Supported H−H Activation by the Metal
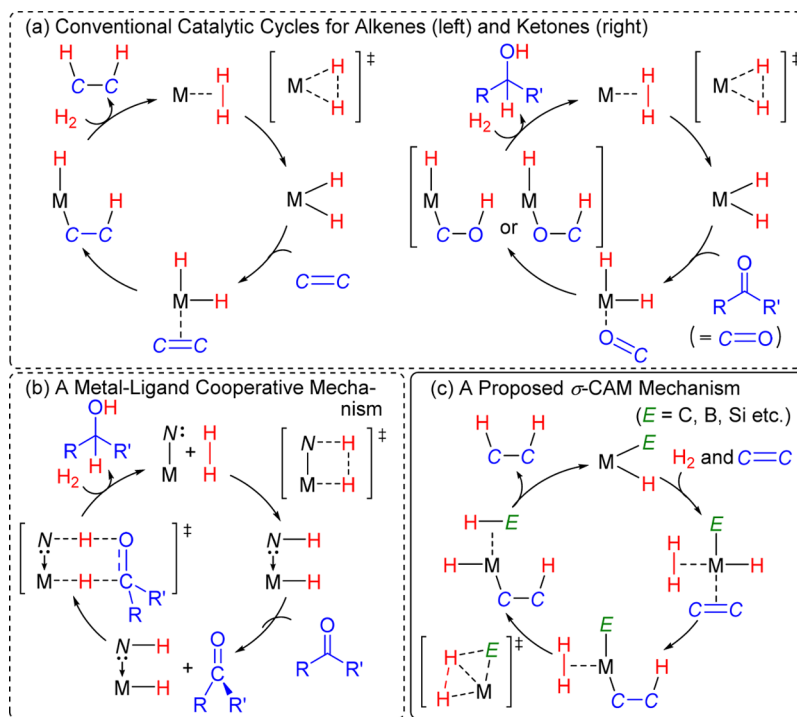
transition metals with a coordinated H−H group forms a η^2-(H−E) moiety and a H−M−alkyl bond that take part in forming the alkane. The potential of the σ-bond metathesis of late transition metals has recently been widely investigated both experimentally and theoretically, and it has been concluded that the reaction can be considered as "oxidative hydrogen migration", a sequence composed of oxidative addition and reductive elimination through a kite-shaped transition state.[4] This is in contrast to the concerted four-membered ring mechanism proposed for the σ-bond metathesis of d^0 transition metal complexes. The involvement of the σ-CAM mechanism in the catalytic hydrogenation of alkenes by certain ruthenium−phosphine complexes was suggested by Perutz and Sabo-Etienne, although no experimental or theoretical studies were undertaken, as far as we are aware.[5]

Due to increasing interest in the development of environmentally benign chemical processes, the iron-catalyzed hydrogenation of unsaturated molecules has received significant attention. Although several iron-catalyzed hydrogenations of ketones[6−9] and alkenes[10−14] have been reported, as shown in Chart 1, to the best of our knowledge, there have been no reports that the associated catalytic cycles unequivocally involve the conventional oxidative addition of H$_2$ to the iron center, as shown in Scheme 1a.[15] In other words, the development of new iron-based hydrogenation catalysts requires a consideration of the manner in which the H−H bond of molecular hydrogen is cleaved during the catalytic cycle. It is apparent that the metal−ligand cooperation mechanism shown in Scheme 1b allows for the efficient iron-catalyzed hydrogenation of carbonyl compounds.[6−9] Typical catalysts that have been reported to date include the pincer-type complexes investigated by Milstein[6] and Guan[7] and an iron homologue of Shvo's catalyst that was assessed by Casey.[8] While iron species tend to have both low- and high-spin states, the majority of these hydrogenation

Chart 1. Selected Examples of Well-Defined Iron Complexes for Catalytic Hydrogenation Reactions[a]
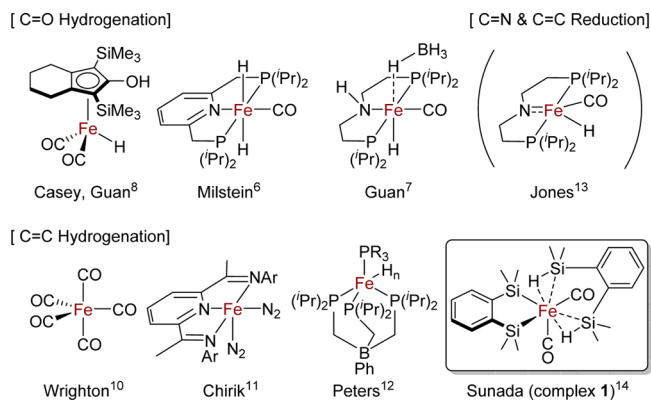

[a]Complex **1** is a proposed structure.

catalysts for carbonyl compounds are in the low-spin state, and evidence for the ligand-assisted H−H cleavage action of these compounds has been provided both experimentally and theoretically.[16]

Among the relatively rare alkene hydrogenation catalysts, studies of three well-defined complexes have included discussions of possible catalytic intermediates.[10−14] One such complex is photoactivated Fe(CO)$_5$, as reported by Wrighton in the 1970s.[10] Although iron carbonyls typically show little catalytic activity even under harsh conditions, continuous photoirradiation can generate catalytically active species that promote the efficient hydrogenation of alkenes, and the possible involvement of triplet (η^2-H$_2$)Fe(CO)$_3$ was suggested by time-resolved IR studies and theoretical calculations. Recent work by Chirik[11] and Peters[12] has demonstrated several iron

Chart 2. Six Possible Isomeric Structures of Complexes 1a–1f
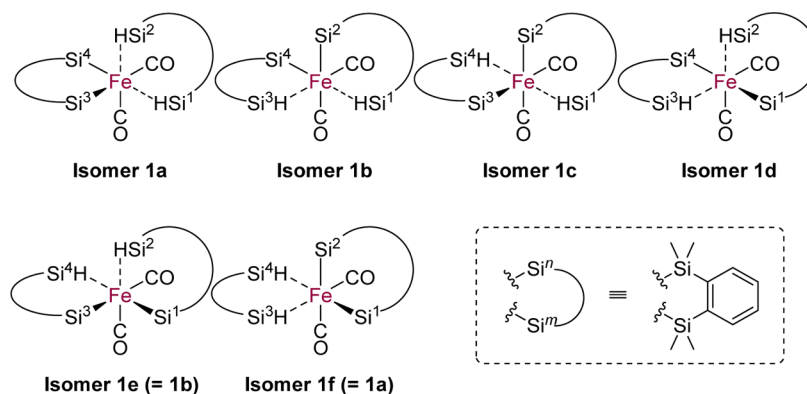
hydrogenation catalysts that are stabilized by bi- or tridentate phosphine, imine, pyridine, and N-heterocyclic carbene ligands. Efforts to isolate possible catalytic intermediates have demonstrated the presence of η^2-H$_2$ intermediates; however, the majority of these were found to be in high-spin states. Further experimental and theoretical studies to elucidate the hydrogenation mechanisms have not yet been performed. With regard to all three of these catalysts, it is important to note that no clear evidence has been obtained regarding the manner in which the H−H bond of the η^2-H$_2$ ligand on the iron is cleaved and subsequently contributes to the catalytic hydrogenation of the alkene. The possibility that the iron-catalyzed hydrogenation of alkenes proceeds by way of a σ-CAM process such as that shown in Scheme 1c has not yet been confirmed, although Peters et al. reported a stoichiometric reaction that involves cleavage of the H−H bond of coordinated molecular hydrogen by an Fe−B bond.[17]

Among the iron catalysts active for the hydrogenation of alkenes, the disilaferracyclic iron carbonyl complex **1** discovered previously by our research group is unique in that it promotes the reaction at room temperature under 1 atm of H$_2$.[14] Since iron carbonyls do not catalyze hydrogenation without photoirradiation under such extremely mild conditions, the mechanism of hydrogenation catalyzed by **1** is of significant interest. The characteristic structural features of **1** are its octahedral geometry and coordination of strong field ligands. The two CO ligands act as strong π-acids, while the two silyl groups are good σ-donors that result in **1** being a low-spin compound. If we assume that these structural features are maintained during the catalysis process, all of the catalytic intermediates could also be in the low-spin state. As recently reported by Chirik and co-workers,[11c] strong field organometallic compounds based on first row transition metals like metal carbonyls are rare but could enable the two-electron chemistry observed in the hydrogenation mechanisms of precious metal catalysts. Furthermore, the presence of two Fe−Si bonds in the catalytic intermediates originating from **1** may activate H−H bonds through Fe−Si/η^2-(H−H) oxidative hydrogen migration. These assumptions prompted us to perform DFT calculations regarding the mechanism of hydrogenation catalyzed by **1**. We first calculated the optimized structures of **1**, which provided unique insights into the nonclassical Si−H coordination with the metal in this compound. The H$_2$FeSi$_4$ framework in **1** was found to be associated with two Si⋯H⋯Si secondary interactions, in which the hydrogen atoms fluctuate around the iron center, with a very low associated energy barrier. The exchange of the

bis(dimethylsilyl)benzene (BDSB) ligands in **1** with ethylene and H$_2$ molecules was determined to generate a catalytically active disilaferracycle bearing η^2-ethylene and η^2-H$_2$ ligands. Further studies of this species elucidated catalytic cycles explained by the σ-CAM mechanism that differ from the original mechanism proposed by Perutz and Sabo-Etienne,[3] as shown in Scheme 1c.

■ RESULTS

Geometrical Optimization of 1. In our previous paper,[14] we proposed that one possible structure of **1**, namely, **1a**, is a disilaferra(II)cycle having two CO and two Si−H ligands, as shown in Chart 2. This structure is reasonable based on the 18 electron rule. X-ray analysis of **1** revealed the octahedral arrangement of the two *cis*-CO ligands and four silyl groups around the iron center (Figure 1a). Unfortunately, the hydrogen atoms that should have been bonded with two of the four Si atoms were not located in the difference Fourier map. The presence of Si−H moieties and *cis*-carbonyl ligands was clearly supported by IR spectroscopy. However, only single
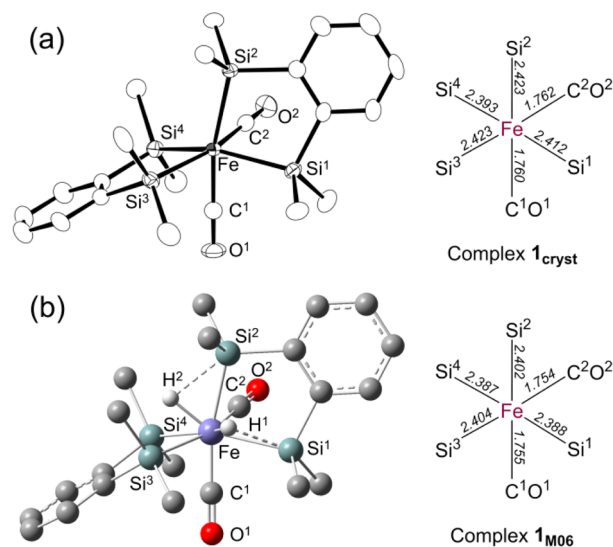

Figure 1. (a) Molecular structure of **1** determined by X-ray analysis (expressed as **1$_{cryst}$**) and the Fe−Si and Fe−C(CO) bond distances (Å). Hydrogen atoms which should be on two of the silicon atoms were not located. (b) Structure of **1** optimized with the M06 calculation (expressed as **1$_{M06}$**) and the Fe−Si and Fe−C(CO) bond distances (Å).

signals were observed in ^{1}H and ^{29}Si NMR spectra acquired in solution, even at low temperatures. This result is inconsistent with the proposed structure for **1a**, which should generate two ^{1}H signals and two [29]Si resonances due to the magnetically inequivalent σ-silyl and Si–H ligands. We attribute this to the rapid equilibrium of **1a** with five other isomeric structures (**1b**, **1c**, **1d**, **1e**, and **1f**), as shown in Chart 2. These structures result from hydrogen transfer between the two Si atoms in the iron coordination sphere via oxidative hydrogen migration between Fe–Si σ-bonds and Si–H ligands. However, no further experimental evidence regarding the location of the hydrogen atoms has been obtained from NMR so far.

The M06 calculations for **1** were performed based on the atomic coordinates of Fe, C, H, O, and Si obtained from the crystal structure of this compound (expressed as **1$_{cryst}$**), in which two hydrogen atoms due to the two Si–H moieties were assumed to be located near the iron center. Interestingly, the optimized structure of **1** (expressed as **1$_{M06}$** and shown in Figure 1b) was found to be different from our expectations. The Fe–Si distances in **1$_{M06}$** are 2.388, 2.402, 2.404, and 2.387 Å, whereas the Fe–C(CO) distances are 1.755 and 1.754 Å. These values are in agreement with the bond distances observed in **1$_{cryst}$**. In addition, the Fe–Si distances are similar to typical Fe–Si σ-bond lengths, such as those found in the disilaferracyclic compounds **2** and **3** rather than those associated with σ-Si–H coordination. Two H atoms bonded with the two Si moieties are found in the **1$_{M06}$** structure; one H atom (H[1]) is located midway between the two Si atoms, Si[1] and Si[3], while the other (H[2]) is centered between Si[2] and Si[4]. All of the Si–H distances calculated are in the range of 2.0 to 2.4 Å, values that are longer than the typical η^1- or η^2-(H–Si) distance of 1.7 to 1.8 Å.[18] Examining these distances in more detail, the Si[1]–H[1] (2.064 Å) and Si[2]–H[2] (2.120 Å) distances are slightly shorter than the Si[3]–H[1] (2.361 Å) and Si[4]–H[2] (2.342 Å) lengths, respectively. The Fe–H[1] (1.531 Å) and Fe–H[2] (1.526 Å) distances are in agreement with reported iron–hydride bond lengths (1.514 to 1.538 Å) as determined by neutron diffraction studies.[19] The Mayer bond order analyses shown in Figure 2a clearly show the presence of two Fe–H σ-bonds (bond order >0.7) as well as four Fe–Si bonds (bond orders =

0.52 to 0.60). Weak bonding interactions can be observed between H and Si atoms (bond orders = 0.03 to 0.11). These results suggest that **1$_{M06}$** has four Fe–Si and two Fe–H bonds with two Si···H···Si interactions or so-called SISHA (secondary interaction between silicon and hydrogen atoms),[3] a structure shown as **1g** in Figure 2b.

While the low-spin singlet ground state of **1$_{M06}$** (**[1]1$_{M06}$**) is computationally predicted, it should be noted that iron complexes tend to be high-spin rather than low-spin. We therefore carried out a geometrical optimization of **1$_{M06}$** with different spin states (triplet (**[3]1$_{M06}$**; S = 1) and quintet (**[5]1$_{M06}$**; S = 2)), as described in Table 1. The optimized **[3]1$_{M06}$** and **[5]1$_{M06}$** structures were found to have trigonal bipyramidal and tetrahedral geometries, respectively, with relatively high energies compared to **[1]1$_{M06}$** [ΔE(**[1]1$_{M06}$**/**[3]1$_{M06}$**) = +27.2 kcal/mol, ΔE(**[1]1$_{M06}$**/**[5]1$_{M06}$**) = +43.6 kcal/mol]. Single-point energy calculations of the triplet and quintet states performed for the **[1]1$_{M06}$** geometry showed additional large energy gaps [ΔE(**[1]1$_{M06}$**/**[3]**{**[1]1$_{M06}$**}) = +61.7 kcal/mol, ΔE(**[1]1$_{M06}$**/**[5]**{**[1]1$_{M06}$**}) = +136.6 kcal/mol]. These results suggest that the high-spin species of **1** are unfavorable compared to the low-spin species.

Further searches for optimized structures of **1** resulted in the identification of four geometrical isomers of **1$_{M06}$**, namely, **1$_{M06}$-2**, **1$_{M06}$-3**, **1$_{M06}$-4**, and **1$_{M06}$-5**, all very close together in energy. In addition, **1$_{M06}$-4** and **1$_{M06}$-5** are equivalent to **1$_{M06}$-2** and **1$_{M06}$**, respectively, as a result of molecular symmetry. The structural features of these isomers stem from differences in the dihedral angles between the plane, including the Fe center and two Si atoms and the plane of the benzene ring in the two disilametallacycle moieties, as shown in Figure 3b. Interconversions among these isomers are possible via flipping of two benzene rings, as portrayed in Figure 3b, which in turn varies the Si···H interactions. As an example, interconversions between structures **1$_{M06}$** and **1$_{M06}$-5** are achieved via the strong Si–H interaction indicated by red lines in Figure 3a, which are weakened, while the weak Si···H interaction indicated by the blue broken line becomes stronger. Similar to **1$_{M06}$**, the bond distances and Mayer bond order analyses of **1$_{M06}$-2**, **1$_{M06}$-3**, **1$_{M06}$-4** (=**1$_{M06}$-2**), and **1$_{M06}$-5** (=**1$_{M06}$**) summarized in the Supporting Information suggest that these structures are homologous to **1g**, which has four Fe–Si and two Fe–H bonds in conjunction with two Si···H···Si interactions. It is noteworthy that the interconversions between **1$_{M06}$** and **1$_{M06}$-5** take place with virtually no energy barrier at room temperature. In other words, it is a special feature of **1** that the hydrogen atoms fluctuate significantly around the iron center.

All of the above results obtained by M06 calculations are consistent with data obtained experimentally. First, the Fe–Si and Fe–C(CO) bond distances of **1** obtained by X-ray diffraction studies (expressed as **1$_{cryst}$**) are almost identical to those of **1$_{M06}$**. Second, NMR spectra of **1** do not exhibit any signal broadening due to the paramagnetism, in agreement with the low-spin state of **1**. Third, the single ^{1}H and ^{29}Si NMR signals generated by **1** even at −90 °C are supported by the isomerization among **1$_{M06}$** to **1$_{M06}$-5** due to the lack of an energy barrier. The fourth piece of evidence is the [29]Si–[1]H coupling constant, which is known to be a good index of the strength of the interaction between the Si and H nuclei.[20] The ^{1}H NMR spectrum of **1** acquired in C_6D_6 exhibits a signal at a δ of −10.2 due to the hydride ligands, with a [29]Si–[1]H coupling constant of $J_{Si–H}$ = 13.2 Hz. In the present work, we simulated the chemical shift of the ^{1}H resonance due to the Si–H group as well as the $J_{Si–H}$ values of three optimized structures, **1$_{M06}$**,
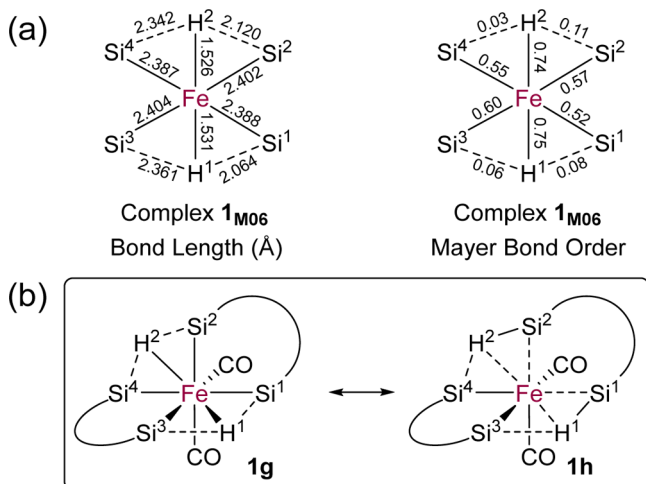

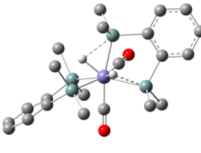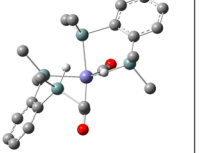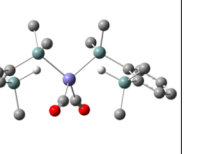**Figure 2.** (a) Selected interatomic distances (Å) and Mayer bond orders for **1$_{M06}$**. (b) **1g** bearing four Fe–Si and two Fe–H bonds with two Si···H···Si weak interactions and **1h** bearing two η^2-(H–Si) ligands, two Fe–Si bonds, and two Si···H weak interactions.

Table 1. Optimized Structure of 1_{M06} with Different Spin States

Complex	$^1 1_{M06}$	$^3 1_{M06}$	$^5 1_{M06}$
Spin state	Singlet	Triplet	Quintet
Optimized structure			
ΔE (kcal/mol)	0.0^a $(0.0)^b$	$+27.2^a$ $(+61.7)^b$	$+43.6^a$ $(+136.6)^b$

$^a\Delta E$ for optimizations of 1_{M06} with different spin states (singlet, triplet, and quintet). $^b\Delta E$ for single-point energy calculations of the triplet and quintet states performed for the $^1 1_{M06}$ geometry.
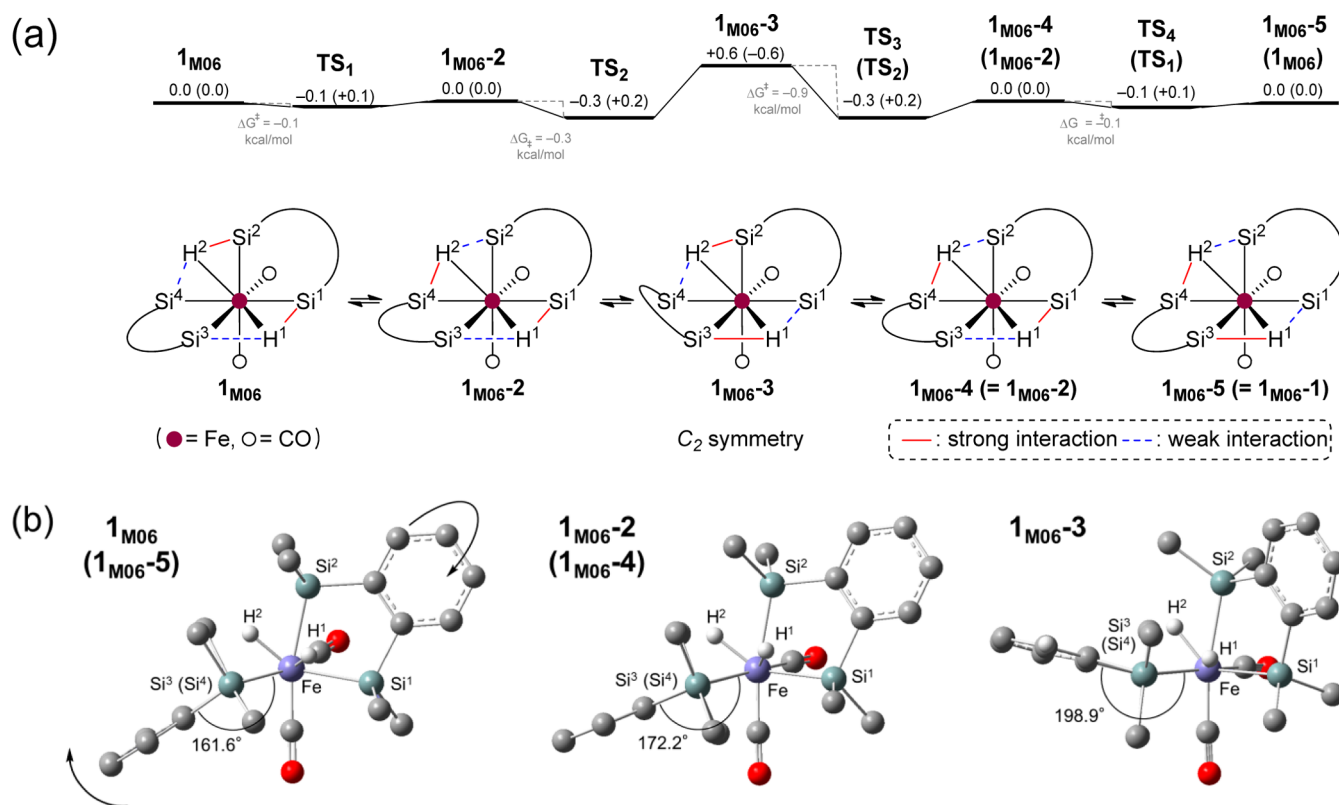
(a)

(b)

Figure 3. (a) Isomerization among 1_{M06}, 1_{M06}-2, 1_{M06}-3, 1_{M06}-4 (=1_{M06}-2), and 1_{M06}-5 (=1_{M06}-1) [ΔG (ΔSCF in parentheses) in kcal/mol]. (b) Optimized structures of 1_{M06} (=1_{M06}-5), 1_{M06}-2(=1_{M06}-4), and 1_{M06}-3.

Table 2. ^{1}H NMR Simulation for a Series of the Isomers of 1 To Calculate δ_H (Fe−H) [ppm] and J_{Si-H} [Hz]

complex	$\delta_H{}^b$ (Fe−H) [ppm]	$|J_{Si-H}|$ for H^1 [Hz]		$|J_{Si-H}|$ for H^2 [Hz]
experimental data	−10.21		13.2	
1_{M06}-1^a (1_{M06}-5)	−10.71(H^1)/−9.91(H^2)	12.2(Si^1)/0.9(Si^3)		9.3(Si^2)/1.8(Si^4)
1_{M06}-2^a (1_{M06}-4)	−10.47(H^1)/−10.45(H^2)	10.2(Si^1)/6.5(Si^3)		7.0(Si^2)/9.6(Si^4)
1_{M06}-3^a	−12.55(H^1)/−12.55(H^2)	11.9(Si^1)/24.6(Si^3)		24.6(Si^2)/11.9(Si^4)

^{a}Conditions: M06/SDD (Fe), 6-31G** (C, H, O, ^{29}Si), NMR = (SpinSpin). ^{b}The values of δ_H are determined by comparison of the isotropic parameter in SCF GIAO magnetic shielding tensor (ppm) between H atoms and tetramethylsilane as a standard.

1_{M06}-2, and 1_{M06}-3, using the spin−spin option of the Gaussian 09 program.[32] As summarized in Table 2, the estimated δ_H(Si−H) values are in the range of −9.9 to −12.6, roughly equal to the experimental value (−10.21). The estimated $|^2J_{Si-H}|$ values are in the range of 6.5 to 24.6 Hz, which are also similar to the actual ^{29}Si−^{1}H coupling constant and much smaller than the typical $|^2J_{Si-H}|$ values of σ-Si−H complexes (40 to 70 Hz). These simulations are also consistent with the results of the

Mayer bond order analyses for 1_{M06}, 1_{M06}-2, and 1_{M06}-3, which indicate weak interactions between Si and H atoms in **1g**, as described in Figure 2b.

Hydrogenation of Ethylene. We next investigated the reaction pathways for the hydrogenation of ethylene as catalyzed by **1**. Since **1** is a coordinatively saturated 18 electron complex, the generation of a coordinatively unsaturated species and the coordination of ethylene and H_2 are necessary to

initiate a catalytic cycle. Two experimental results provided clues when considering this coordinatively unsaturated species: free BDSB is formed during the catalytic reaction, and the reaction of **1** with 2,6-dithiaheptane gives both complex **3** and BDSB.[14] These findings are interpreted as the result of the dissociation of BDSB from **1** to give a disilaferracycle moiety having two carbonyl ligands and a 14 electron configuration. This species is able to react with ethylene and H$_2$ to generate **A1** and its isomer **B1**, as shown in Scheme 2a.

Scheme 2. (a) Formation of A1/B1 from 1 and (b) Plausible Catalytic Cycle for the Hydrogenation of Ethylene Starting from A1 or B1, Involving Oxidative Hydrogen Migration between η^2-H$_2$ Species and an Fe−Si Bond (Step 1), Hydrogen Migration from the Fe Atom to the η^2-Ethylene Ligand (Step 2), and Formation of Ethane with Regeneration of a Disilaferracyclic Species (Step 3)
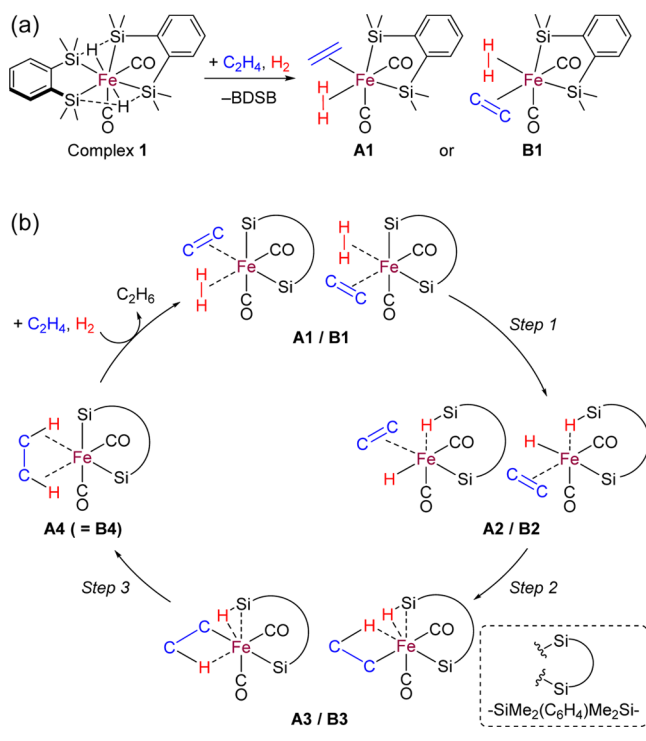
As described in the Introduction, hydrogenation mechanisms catalyzed by noble metals are conventionally explained by catalytic cycles involving oxidative addition of H$_2$, insertion of the C=C moiety of the alkene between the resulting M−H bond, and reductive elimination of the corresponding alkane. However, one plausible mechanism for the hydrogenation of ethylene starting from **A1/B1** differs from the conventional catalytic cycles, as shown in Scheme 2b. This proposed catalytic cycle involves four elementary steps. In step 1, the coordinated H$_2$ in **A1/B1** is cooperatively cleaved by a silyl group of BDSB in conjunction with the iron center to afford **A2/B2**, bearing an agostic Si−H moiety and an Fe−H group. In step 2, hydrogen migration from the iron center to the ethylene ligand leads to the formation of **A3/B3** with a β-agostic Fe−Et moiety. In step 3, the remaining hydrogen bonded to the silyl group migrates to the ethyl group to give the ethane complex **A4/B4**, where **B4** is equivalent to **A4**. Finally, the initial complexes **A1/B1** are regenerated by exchange of the ethane ligand for incoming

molecules of ethylene and dihydrogen. Each step is explained below.

Generation of A1/B1. The M06 calculations provided two optimized structures, **A1** and **B1**, both of which are presented in Figure 4. In **A1**, the η^2-H$_2$ ligand is *trans* to the C^{2}O^2 ligand,
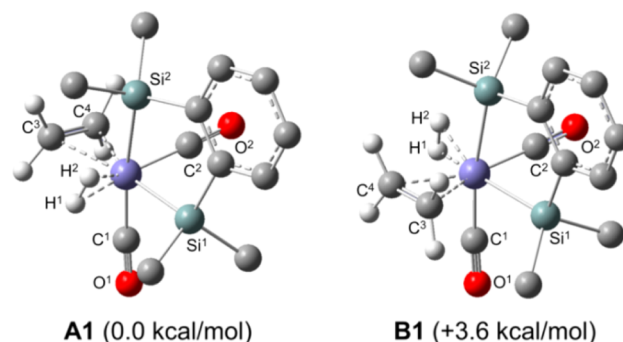

Figure 4. Optimized structures of **A1** and **B1** calculated with the M06 functional.

whereas the η^2-ethylene is in the *trans* position relative to the Fe−Si^1 σ-bond. **B1** is an isomer of **A1** in which η^2-H$_2$ is *trans* to the Fe−Si^1 σ-bond and ethylene is *trans* to the C^{2}O^2 ligand. **B1** is higher in energy than **A1** by $\Delta G°_{A1/B1} = +3.6$ kcal/mol, and the free energy change for the reaction from **1** + C$_2$H$_4$ + H$_2$ to **A1** + BDSB is endergonic, with a value of +7.8 kcal/mol. It is noteworthy that, for both **A1** and **B1**, the ethylene ligand is in a plane containing Fe, Si^1, C^2, and O^2 atoms. In contrast, the H−H axis is parallel to the axis containing O^1, C^1, Fe, and Si^2, and the Fe−Si^1−C^1 plane bisects the H−H bond. The H−H distance is 0.869 Å for both **A1** and **B1**, which is longer than the uncoordinated H−H bond length by 0.12 Å. In contrast, the C=C distance is 1.377 Å (**A1**) and 1.383 Å (**B1**), which is longer than that of free ethylene by 0.05 Å. These values indicate back-donation from iron to the σ*-orbital of the η^2-H$_2$ ligand and the π*-orbital of the η^2-ethylene moiety. Since the catalytic cycle starting from **A1** is very similar to that from **B1**, the **A1** mechanism is described below for steps 1, 2, and 3. In the following sections, we first discuss the reaction pathways starting from **A1**, while those beginning with **B1** are discussed further on.

Step 1. Cleavage of the H−H Bond Assisted by the Fe−Si σ-Bond. As described in the Introduction, conventional hydrogenation mechanisms are initiated by the oxidative addition of H$_2$ to the metal center. The attempted oxidative addition of the coordinated H$_2$ to the iron center of **A1** results in H−H cleavage assisted by the adjacent Fe−Si σ-bond, which occurs in conjunction with a surprisingly small activation energy (Figure 5). The conversion of **A1** to **A2** is isoenergetic ($\Delta G°_{A1/A2} = -0.2$ kcal/mol) with an activation Gibbs free energy of $\Delta G^{\ddagger} = 2.6$ kcal/mol. The η^2-H$_2$ ligand in **A1** is coplanar with the Fe−Si^2 σ-bond, and the distance between the Si^2 atom and H^2 atom of the η^2-H$_2$ ligand is 2.270 Å. These conditions are well-suited to oxidative hydrogen migration leading to a change from the H^1−H^2/Fe−Si^2 coordination mode to the Fe−H^1/Si^2−H^2 mode. The structure of **TS$_{A1/A2}$** clearly demonstrates the transfer of H^2 from a position close to H^1 to one near the Si^2 in the Fe−Si^2−H^2−H^1 plane, accompanied by elongation of the H^1−H^2 and Fe−Si^2 bonds and shortening of the H^2−Si^2 bond.[21] The bond length and bond order of the Fe−H^2 bond in **TS$_{A1/A2}$** are 1.521 Å and 0.62, respectively, suggesting that the reaction is a typical
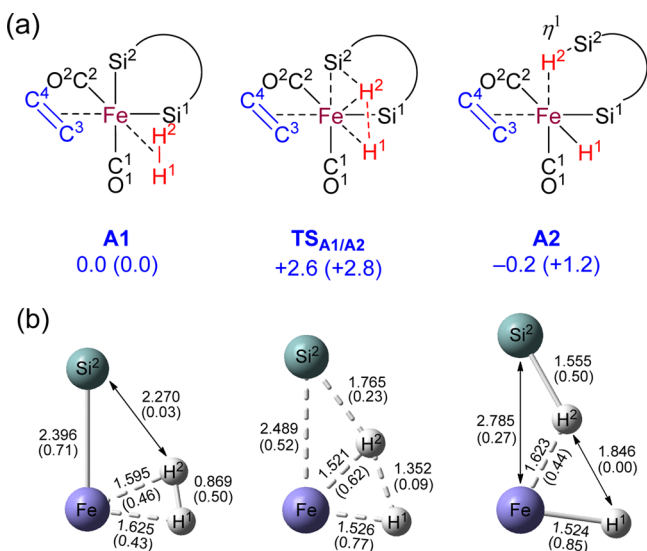
Figure 5. (a) Transformation of **A1** to **A2** [ΔG (ΔSCF in parentheses) in kcal/mol]. (b) Selected interatomic distances of **A1**, **TS$_{A1/B1}$**, and **B1** [Å] and their Mayer bond orders in parentheses.

oxidative hydrogen migration via a kite-shaped, four-membered ring transition state. Typically, there is no M−H^2 interaction in four-membered transition states associated with the M−Si/M−(η^2-H^1−H^2) σ-bond metathesis of d^0 transition metals.[22]

Step 2. Hydrogen Atom Migration to Ethylene. The resulting **A2** has an Fe−H bond and an agostic Si−H ligand. The optimized structure of **A2** suggests that the agostic Si−H ligand should be described as η^1-(H−Si). The Fe−H σ-bond of **A2** is coplanar with the C=C bond of the ethylene ligand, promoting migration of the hydrogen atom on the Fe atom to the carbon in the coordinated ethylene. This step corresponds to insertion of a C=C bond between an M−H bond, a step that is typically included in conventional explanations of catalytic hydrogenation. Figure 6 shows this hydrogen migration process, including the conversion of **A2** to the Et−Fe species **A3-η^1** through a four-membered ring transition state
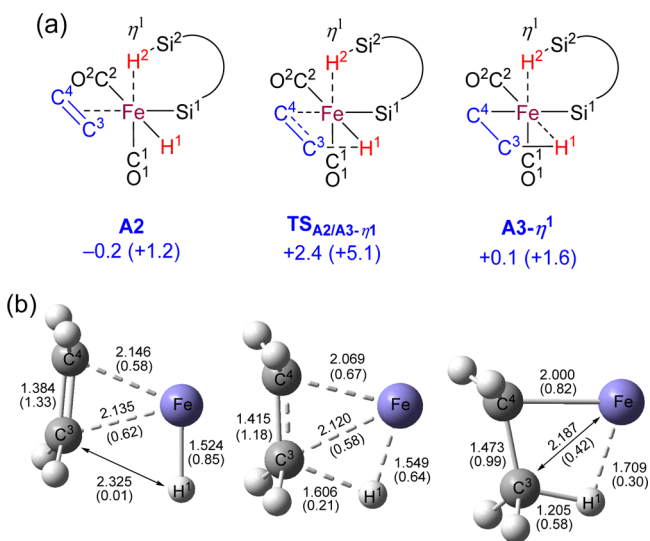

Figure 6. (a) Transformation of **A2** to **A3-η^1** [ΔG (ΔSCF in parentheses) in kcal/mol]. (b) Selected interatomic distances of **A2**, **TS$_{A2/A3-\eta^1}$**, and **A3-η^1** [Å] and their Mayer bond orders in parentheses.

consisting of Fe, C^4, C^3, and H^1. There is essentially a zero energy gap ($\Delta G^{\circ}_{A2/A3-\eta^1}$ = +0.3 kcal/mol) between **A2** and **A3-η^1**, and $\Delta G^{\ddagger}$ is also very small (2.6 kcal/mol). The transition state structure shows that increasing interaction between H^1 with C^3 gives rise to elongation of the C^3−C^4 bond and formation of a β-agostic C−H bond.

Step 3. Formation of Ethane with Regeneration of the Fe−Si Bond. Two notable structural features are found in **A3-η^1** in Figure 6: a η^1-(H−Si) ligand and an β-agostic C−H bond. Three conformational isomers of **A3-η^1** are possible, two of which possess the η^1-(H−Si) moiety, **[A3-η^1]′** and **[A3-η^1]′′**, and the other with a η^2-(H−Si) moiety, **A3-η^2**. As summarized in the Supporting Information, interconversions among these four species are isoenergetic (ΔG° < 3.3 kcal/mol) with an activation Gibbs free energy of $\Delta G^{\ddagger}$ < 1.7 kcal/mol. The final step of the catalytic cycle is hydrogen migration from the η^2-(H−Si) ligand in **A3-η^2** to the σ-carbon of the ethyl ligand. This corresponds to the elimination of ethane from the Fe(II) center. In **A3-η^2**, Si^2, H^2, and C^4 are bonded to the iron center, and these four atoms are in the same plane. This is amenable to the generation of a four-membered transition state, **TS$_{A3-\eta^2/A4}$**. The transition from **A3-η^2** to **A4** is exergonic ($\Delta G^{\circ}_{A3-\eta^2/A4}$ = −14.4 kcal/mol) with a very low activation energy of 1.5 kcal/mol (Figure 7). The structure of the transition state **TS$_{A3-\eta^2/A4}$**
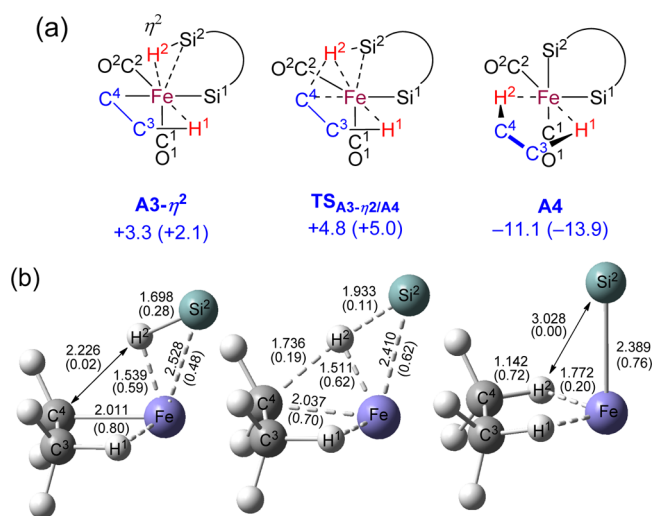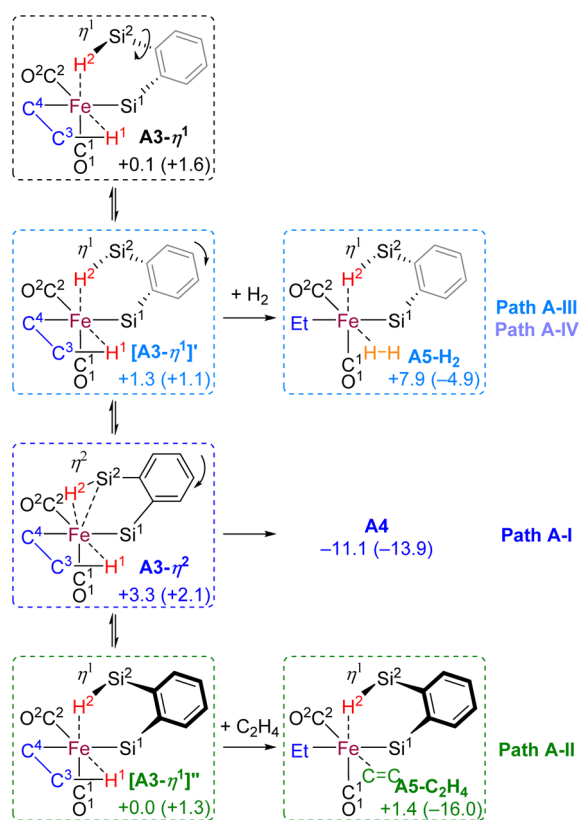

Figure 7. (a) Transformation of **A3-η^2** to **A4** [ΔG (ΔSCF in parentheses) in kcal/mol]. (b) Selected interatomic distances of **A3-η^2**, **TS$_{A3-\eta^2/A4}$**, and **A4** [Å] and their Mayer bond orders in parentheses.

demonstrates that the transfer of H^2 from Si^2 to C^4 takes place while maintaining the β-agostic C^3−H interaction of the Fe−ethyl moiety and also while maintaining a strong interaction between H^2 and the Fe center. This process also represents a typical oxidative hydrogen migration, just as seen in step 1.

The elimination of ethane to form **A4** is accompanied by the formation of an Fe−Si bond to regenerate the disilaferracyclic structure seen in **A1**. Since the coordination of ethane in **A4** is weak, the replacement of ethane by ethylene and H$_2$ results in the regeneration of **A1** to complete the catalytic cycle. The process from **A4** to **A1** is exergonic (ΔG° = −15.0 kcal/mol).[23]

Alternative Pathways. We also calculated three alternative catalytic cycles, the first of which is that in step 3. The loss of the β-agostic interaction of the ethyl group in **A3-η^1** and its isomers allows an ethylene or H$_2$ molecule to be coordinated to the resulting vacant site. As shown in Scheme 3, the reaction of

Scheme 3. Alternative Pathways A-I, A-II, A-III, and A-IV [ΔG (ΔSCF in parentheses) in kcal/mol]

formation of ethane is small in path A-III (−0.06 kcal/mol) but relatively high (4.0 kcal/mol) in path A-IV. These alternative pathways for the formation of ethane are less favorable in terms of energy than the direct formation of ethane (path A-I) described in the former paragraph. More details regarding these deliberations are provided in the Supporting Information.

The second alternative pathway starts from **B1**, an isomer of **A1**. The hydrogenation of ethylene beginning with **B1** proceeds in a manner similar to that from **A1**, by way of (1) oxidative hydrogen migration from a η^2-H$_2$ species to an Fe−Si bond, (2) hydrogen migration from the Fe atom to the η^2-ethylene ligand, and (3) elimination of ethane to form a disilaferracyclic species, with regeneration of **B1** by replacement of the coordinated ethane by ethylene and H$_2$, as detailed in the Supporting Information. Although **B1** is 3.6 kcal/mol higher in energy than **A1**, the ethyl−Fe intermediate **B3-η^1** formed by hydrogen migration to the η^2-ethylene ligand is 4.3 kcal/mol lower than **A3-η^1**. In contrast to **A3-η^1**, the change of the coordination mode from η^1-H−Si to η^2-H−Si in **B3-η^1** proceeds in one step. It should be noted that the activation energy associated with the elimination of ethane is relatively high (+4.9 kcal/mol). In summary, the hydrogenation pathway from **B1** is somewhat less favorable compared to that beginning from **A1** with respect to energy, although each individual step in this process has a low energy barrier (<5 kcal/mol).[24]

The third possibility involves alternative spin states starting from **A1** or **B1**. As described above, **1** in the high-spin state is apparently unfavorable. In the calculations so far described, all of the intermediates and transition states were therefore low-spin. We performed single-point energy calculations for intermediates in the triplet and quintet spin states and found that a significant high-spin/low-spin state energy gap exists for the same structures of each species (see details in the Supporting Information). This supports our initial assumption that the catalytic cycle for the hydrogenation of ethylene using **1** as a precatalyst consists of low-spin intermediates and transition states similar to those associated with noble metal catalysts. Total relative energy diagram of two reaction pathways from **A1** and **B1** for hydrogenation of ethylene are summarized in Scheme 4.

■ DISCUSSION

Mechanistic Considerations. *Optimized Structures of 1.* The nonclassical coordination of H−H,[25] C−H,[26] and Si−H[18]

[**A3-η^1**]″ with ethylene produces the ethyl complex **A5-C$_2$H$_4$**, and migration of the hydrogen atom of the η^1-(H−Si) moiety to the α-carbon of the ethyl group results in the formation of ethane and regeneration of a disilaferracycle (path A-II). The coordination of H$_2$ to [**A3-η^1**]′ forms **A5-H$_2$**, which provides two possible pathways to the formation of ethane. These are hydrogen migration to the ethyl group either from the η^1-(H−Si) moiety (path A-III) or from the η^2-H$_2$ ligand (path A-IV). In the case of path A-II, the coordination of ethylene is slightly endergonic ($\Delta G° = +1.4$ kcal/mol), although the $\Delta G^{\ddagger}$ value of the C−H bond formation is relatively high (+7.5 kcal/mol). In the latter two processes, the formation of the η^2-H$_2$ intermediate is endergonic by +6.6 kcal/mol. The $\Delta G^{\ddagger}$ of the

Scheme 4. Relative Energy Diagram of Two Reaction Pathways from A1 (blue line) or B1 (red line) for Hydrogenation of Ethylene [ΔG (ΔSCF in parentheses) in kcal/mol]
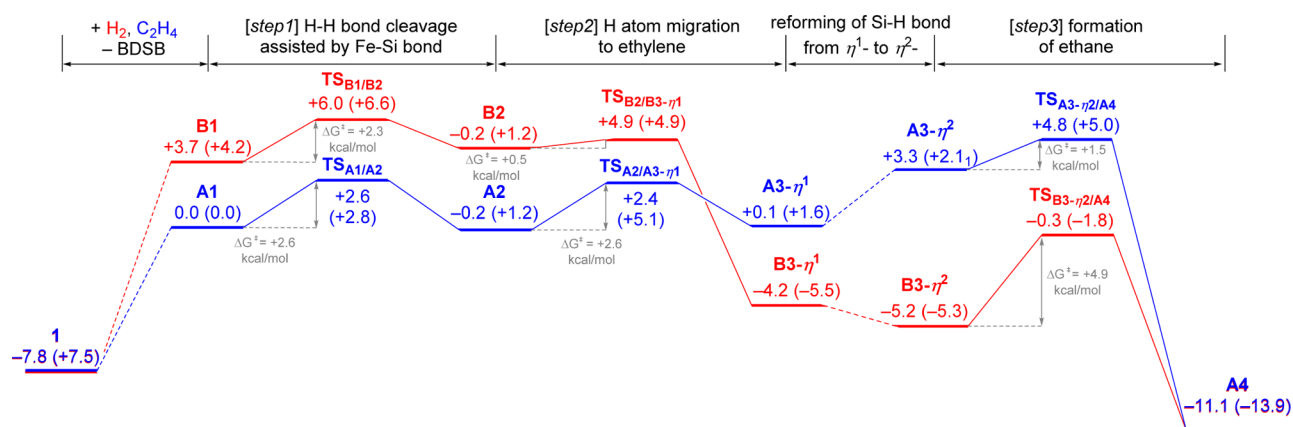
moieties have been discussed in recent reviews of organometallic chemistry and are important with regard to the present discussion. Representative nonclassical Si−H coordination modes are shown in Figure 8, as classified by Corey. The

Figure 8. Typical Si−H bond distances (Å) and J_{Si-H} (Hz) of uncoordinated Si−H (A) and classical and nonclassical Si−H interactions with metal (B to E).

geometric optimization of **1** using the M06 functional generates several structural isomers, all of which are best described as a tetrasilyl−dihydride iron complex with secondary interactions (see the SISHA in Figure 8). Although hexavalent iron is unusual in organoiron chemistry, this result could be explained by the characteristically strong σ-donor properties of the organosilyl and hydrido ligands, which tend to stabilize a higher valence metal center.[27] In fact, the closely related complex Ru(IV)HSi$_3$, in which organosilyl and hydrido ligands stabilize a higher valence metal species, was recently reported by Sabo-Etienne et al.[28] Both Si$_2$H and Si$_3$H SISHA interactions are suggested by the Si−H bond distances determined by X-ray or neutron diffraction and the J_{Si-H} value of 9.0 Hz.

Facile interconversion among the various isomers of **1** is suggested by experimental data, especially the singlet ^{29}Si resonance observed in solution at low temperature, and is also supported by DFT calculations. The isomers of **1$_{M06}$** and **1$_{M06-2}$** to **1$_{M06-5}$** have a Si$_4$FeH$_2$ framework with two Si···H···Si SISHA. The interconversion among these isomers occurs with virtually no energy barrier and is accompanied by small movements (or fluctuations) of the hydrogen atoms and variations in the bonding interactions between Si and H atoms (Figure 3). Although the following discussion carefully considers the accuracy of the computational level employed in the present study, it is worth pointing out that the Si···H···Si SISHA in **1$_{M06}$** is unsymmetrical. In Figure 2a, the differences in the two Si−H bond lengths are 0.222 Å for H^1 and 0.297 Å for H^2, whereas those in the Si−H bond orders are 0.08 and 0.02, respectively. These values imply that **1$_{M06}$** may be interpreted as the structure **1g** with some contribution of **1h** (Figure 2b).

Of interest is that these calculations do not necessarily rule out the possible existence of the isomers originally proposed in our previous paper. Although our attempted optimization of **1a** to **1f** did not converge, the associated single-point energy calculations suggest that the energies of these species are only slightly higher than that of **1$_{M06}$**. This result suggests a reasonable scheme for the generation of the catalytically active species **A1** and **B1** from **1$_{M06}$** by way of **1a**, having two weakly coordinated Si−H moieties in a BDSB ligand that undergo ligand exchange with H$_2$ and ethylene.

Catalytic Cycles. The M06 calculations produced the catalytic cycles shown in Scheme 2. The generation of **A1** or **B1** from **1$_{M06}$** is reasonably supported by the small energy difference between the precursor and the product. The energy

diagram (Scheme 3) by way of steps 1 to 3 suggests that the pathway from either **A1** or **B1** proceeds with a low energy barrier (ΔG < 5 kcal/mol). Of particular importance is that all of the catalytic intermediates and transition states are in the low-spin state, as a result of the optimized catalyst structure with octahedral geometry and strong ligand field ligands (π-acidic CO ligands) and σ-silyl moieties as strong σ-donors.

Further contributions of the octahedral geometry to the catalytic cycle are evident in the smooth reactions of steps 1 to 3. In the case of both **A1** and **B1**, the H−H axis of the η^2-H$_2$ moiety is parallel to the Fe−Si σ-bonds, whereas the C−C bond of the η^2-ethylene ligand is perpendicular relative to one Fe−Si σ-bond and coplanar with the other Fe−Si σ-bond. The former contributes to the facile Fe−Si/H−H oxidative hydrogen migration to form an Fe−H σ-bond and a η^2-(H−Si) moiety in **A2** and **B2** to complete step 1. Since the resulting Fe−H σ-bond is coplanar with the η^2-ethylene ligand, facile hydrogen atom migration from the iron atom to one carbon atom of the η^2-ethylene ligand occurs to give the β-agostic ethyl group in **A3-η^1** and **B3-η^1** (step 2). After a change in the coordination mode of the agostic Si−H ligand, the octahedral geometry of **A3-η^2** and **B3-η^2** also contributes to step 3 by allowing facile oxidative hydrogen migration leading to a change of the coordination mode from η^2-Si−H/Fe−C σ-bond to Fe−Si σ-bond/η-C−H. As described above, the interconversion among the isomers of **1$_{M06}$** is accompanied by the fluctuation of hydrogen atoms around the iron center, with accompanying variations in the strength of the Si−H interactions. Similar fluctuations of the hydrogen atoms leading to a transfer of hydrogen atoms among the Fe, Si, and C atoms takes place in the catalytic cycle, with a minimal associated energy barrier, and play a crucial role in promoting the ready hydrogenation of ethylene. The Fe−H bond distances and bond orders suggest that these fluctuations proceed throughout the oxidative hydrogen migration process.

The calculated catalytic cycles shown in Scheme 2 can be considered to be σ-CAM mechanisms in the sense that cleavage of the H−H bond of a coordinated H$_2$ ligand is assisted by an adjacent metal−silicon bond and σ-bond metathesis based on late transition metals (equivalent to oxidative hydrogen migration). However, these cycles are also evidently different from the original mechanism proposal by Perutz and Sabo-Etienne and illustrated in Scheme 1c.[3] This prior scheme begins with an H−M−E species, and H−H/M−E oxidative hydrogen migration is only involved in one step of the reductive elimination of ethane from the metal center. Our calculations suggest that a σ-CAM mechanism is involved in both activation of the H−H bond of the η^2-H$_2$ moiety by an Fe−Si σ-bond and in elimination of ethane by the η^2-Si−H/Fe−C oxidative hydrogen migration.

Comparison with the Mechanisms Involving ^{3}Fe(CO)$_3$. Finally, we include here an argument against the criticism that iron carbonyl species produced by the decomposition of **1** may be responsible for the alkene hydrogenation. Complex **1** has been found to efficiently catalyze the hydrogenation of 1-octene under mild conditions, with a turnover number of 400.[14] However, **1** was not robust during the hydrogenation reaction, and the concurrent formation of brown precipitates that generated CO absorption peaks in IR spectroscopy and did not provide any activity toward the hydrogenation was observed. Wrighton and co-workers have reported the photocatalyzed hydrogenation of alkenes,[10a] in which the photoirradiation of Fe(CO)$_5$ produces catalytically active species containing

$Fe(CO)_3$. Therefore, one could propose that $Fe(CO)_3$ species could possibly result from **1** by decomposition and redistribution of the CO ligands, although we consider this to be unlikely for the following reasons. First, hydrogenation catalyzed by $Fe(CO)_5$ requires continuous photoirradiation to maintain the catalytic activity, due to the ready re-formation of $Fe(CO)_5$ from the unstable $Fe(CO)_3$. Second, we confirmed that the hydrogenation of α-methylstyrene was efficiently catalyzed by **1**. In contrast, Wrighton et al. determined that $Fe(CO)_5$ showed no catalytic activity for this hydrogenation under photoirradiation, a result that our group also confirmed experimentally.[29]

It should also be noted that the hydrogenation of ethylene catalyzed by $Fe(CO)_3$ was also investigated theoretically. BP86 calculations by Weitz and co-workers showed that three intermediates, $(\eta^2\text{-}H_2)Fe(CO)_3$, $(\eta^2\text{-}H_2)(\eta^2\text{-}C_2H_4)Fe(CO)_3$, and $HFe(C_2H_5)(CO)_3$, were obtained,[30a] and these compounds have been identified via time-resolved IR studies of photogenerated species from $Fe(CO)_5$.[30b] However, no reasonable explanation was provided for this cleavage of the H—H bond. Asatryan and co-workers have recently reported detailed calculations using the B3LYP functional and discussed possible mechanisms for the hydrogenation of ethylene, in which the total energy barrier for the catalytic cycle reached as high as 10.4−18.1 kcal/mol.[31]

CONCLUSION

The present paper presents optimized structures determined for the disilaferracyclic complex **1** as well as possible catalytic cycles using **1** as the precatalyst, obtained on a theoretical basis. Our calculations identified the positions of hydrogen atoms bonded with the iron center, which were found to differ from the expected locations.[14] Complex **1** should therefore not be described as having the structure of **1a**, as proposed previously, but rather regarded as the species shown as **1g** with some contribution of **1h**, in which two H and four Si atoms are bonded to the iron center with relatively large bond orders and in which secondary Si···H···Si interactions exist. The replacement of a BDSB ligand in **1** by H_2 and ethylene gives the species **A1** and **B1** in the catalytic cycle, and hydrogenation proceeds by way of steps 1 to 3 having minimal energy barriers, as shown in Schemes 2 and 3. Of particular importance is that all of the catalytic intermediates and transition states calculated were in the low-spin state, and that the octahedral geometry of this species contributes to the three elementary reaction steps for the catalytic hydrogenation of alkenes: H—H cleavage, insertion of a C=C moiety into the Fe—H bond, and the formation of ethane. The activation of H_2 and the formation of ethane, which are generally accomplished by oxidative addition and reductive elimination in the case of catalysis by noble metals, are achieved by σ-CAM mechanisms different from that proposed by Perutz and Sabo-Etienne.[3] These calculation outcomes are in accord with various experimental results, such as the J_{Si-H} constant of **1** and the observation that catalytic hydrogenation proceeds at room temperature under 1 atm of H_2. The present study provides the first theoretical evidence that the σ-CAM mechanism has applications to the actual catalytic hydrogenation of alkenes. This was initially realized by our catalyst design consisting of an octahedral geometry and the introduction of strong ligand field ligands that make possible low-spin intermediates and Fe—Si cooperation. As described in the Introduction, the iron-catalyzed hydrogenation of unsaturated molecules has to overcome the spin problem

associated with the iron center and requires a unique approach to cleaving the H—H bond of coordinated H_2 molecules. Additional studies related to the development of new iron catalysts for hydrogenation based on our catalyst design are currently in progress.

EXPERIMENTAL SECTION

General Procedure. All reactions were performed in a N_2-filled glovebox. Complex **1** was prepared according to the literature.[14] Conversions of 1-octene and α-methylstyrene as well as yields of octane and cumene were determined by ^{1}H NMR spectroscopy (600 MHz) by using anisole as an internal standard. Photoirradiation was performed by 400 kW high-pressure mercury lamp.

Hydrogenation of α-Methylstyrene Catalyzed by 1 or $Fe(CO)_5$. To a 20 mL Schlenk flask equipped with a greaseless valve were placed α-methylstyrene (129.9 μL, 1.00 mmol), complex **1** (24.9 mg, 0.05 mmol), and toluene (0.5 mL). The atmosphere was replaced by H_2 gas, and the solution was stirred at ambient temperature for 6 h. After the reaction, anisole (108 μL, 1.00 mmol) was added. ^{1}H NMR showed that cumene was obtained as a single product (>99%). Photoirradiation of a mixture of α-methylstyrene (129.9 μL, 1.00 mmol), $Fe(CO)_5$ (6.8 μL, 0.05 mmol), and toluene (0.5 mL) under hydrogen atmosphere for 6 h resulted in quantitative recovery of α-methylstyrene.

Hydrogenation of a Mixture of 1-Octene and α-Methylstyrene Catalyzed by 1 or $Fe(CO)_5$. To a 20 mL Schlenk flask equipped with a greaseless valve were placed 1-octene (78.5 μL, 0.50 mmol), α-methylstyrene (65.0 μL, 0.50 mmol), complex **1** (24.9 mg, 0.05 mmol), and toluene (0.5 mL). The atmosphere was replaced by H_2 gas, and the solution was stirred at ambient temperature for 6 h. After the reaction, anisole (108 μL, 1.00 mmol) was added. ^{1}H NMR showed that octane and cumene were obtained (>99%). Photo-irradiation of a mixture of 1-octene (78.5 μL, 0.50 mmol), α-methylstyrene (65.0 μL, 0.50 mmol), $Fe(CO)_5$ (6.8 μL, 0.05 mmol), and toluene (0.5 mL) was carried out at room temperature for 6 h under hydrogen atmosphere. A part of 1-octene was converted to octane (21% conversion), whereas no hydrogenation of α-methylstyrene was observed.

Computational Details. *General Methods.* All of the calculations were performed to search for all intermediates and transition structures on potential energy surfaces using the Gaussian 09 program.[32] For optimization, the M06 functional[33] was selected for the reason described below. We also employed the SDD (Stuttgart/Dresden pseudopotentials)[34] and 6-31G** basis sets[35] for Fe atoms and the other atoms, respectively [**BS1**]. All stationary point structures were found to have the appropriate number of imaginary frequencies. An appropriate connection between a reactant and a product was confirmed by intrinsic reaction coordinate (IRC)[36] and quasi-IRC (qIRC) calculations. In the quasi-IRC calculation, the geometry of a transition state was at first shifted by perturbing the geometries very slightly along the reaction coordinate and released for equilibrium optimization. To determine the energy profile of the proposed catalytic cycle, we performed single-point energy calculations at the optimized geometries using the SDD and 6-311+G**[37] basis sets for Fe atoms and the other atoms, respectively [**BS2**], where solvent effects of THF (ε = 7.4257) were evaluated using the polarizable continuum model.[38] Energy profiles of the calculated reaction pathways are presented as Gibbs free energy changes (ΔG) involving thermal corrections at 298.15 K. Spin−spin coupling constants were computed during an NMR job via the SpinSpin option by using the GIAO method.[20]

Selection of Functionals. Selection of functionals was carried out based on comparison of the crystal structures of two disilaferracycles **2**[39] and **3**[14] shown in Chart 3 with their optimized structures obtained by using six functionals, B3LYP,[40] B3LYP-D,[41] B3LYP*,[42] B3PW91,[43] B97D,[44] and M06.[33] As summarized in the Supporting Information, the Fe−Si and Fe−C(CO) bond lengths of **2** determined by crystallography were similar to those optimized with M06 and B3LYP-D, and those of **3** were the best agreement with the bond

Chart 3. Molecular Structures of 2[39] and 3[14]

Complex **2**   Complex **3**
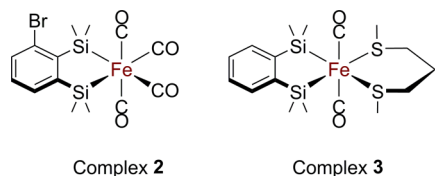
distances optimized with M06. From these results, we selected M06 for the calculations described below.[45]

ASSOCIATED CONTENT

Supporting Information

The Supporting Information is available free of charge on the ACS Publications website at DOI: 10.1021/acs.joc.6b01961.

> Determination of functionals, isomers of **1** and their isomerization processes, details of hydrogenation of ethylene, calculations using B3LYP-D, optimized geometries in XYZ file format and actual charts (PDF)

AUTHOR INFORMATION

Corresponding Author

*E-mail: nagasima@cm.kyushu-u.ac.jp.

Notes

The authors declare no competing financial interest.

ACKNOWLEDGMENTS

REFERENCES

(1) (a) Blaser, H.-U.; Spindler, F.; Thommen, M. In *The Handbook of Homogeneous Hydrogenation*; de Vries, J. G., Elsevier, C. J., Eds.; Wiley-VCH: Weinheim, Germany, 2007. (b) Chaloner, P. A.; Esteruelas, M. A.; Joó, F.; Oro, L. A. *Homogeneous Hydrogenation*; Springer Science & Business Media: Berlin, 2013. (c) Hartwig, J. *Organotransition Metal Chemistry: From Bonding to Catalysis*; University Science Books: Mill Valley, CA, 2009; Chapter 15.

(2) (a) Ohkuma, T.; Ooka, H.; Hashiguchi, S.; Ikariya, T.; Noyori, R. *J. Am. Chem. Soc.* **1995**, *117*, 2675−2676. (b) Noyori, R.; Ohkuma, T. *Angew. Chem., Int. Ed.* **2001**, *40*, 40−73. (c) Noyori, R. *Angew. Chem., Int. Ed.* **2002**, *41*, 2008−2022. (d) Noyori, R.; Kitamura, M.; Ohkuma, T. *Proc. Natl. Acad. Sci. U. S. A.* **2004**, *101*, 5356−5362. (e) Ito, M.; Ikariya, T. *Chem. Commun.* **2007**, *48*, 5134−5142. (f) Abdur-Rashid, K.; Clapham, S. E.; Hadzovic, A.; Harvey, J. N.; Lough, A. J.; Morris, R. H. *J. Am. Chem. Soc.* **2002**, *124*, 15104−15118. (g) Hamilton, R. J.; Bergens, S. H. *J. Am. Chem. Soc.* **2008**, *130*, 11979−11987.

(3) (a) Perutz, R. N.; Sabo-Etienne, S. *Angew. Chem., Int. Ed.* **2007**, *46*, 2578−2592. (b) Lachaize, S.; Sabo-Etienne, S. *Eur. J. Inorg. Chem.* **2006**, *2006*, 2115−2127.

(4) (a) See ref 1c, Chapter 6.5, pp 285−286. (b) Oxgaard, J.; Goddard, W. A., III. *J. Am. Chem. Soc.* **2004**, *126*, 442−443. (c) Oxgaard, J.; Muller, R. P.; Goddard, W. A., III; Periana, R. P. *J. Am. Chem. Soc.* **2004**, *126*, 352−363. (d) Tenn, W. J.; Young, K. J. H.; Bhalla, G.; Oxgaard, J.; Goddard, W. A., III.; Periana, R. P. *J. Am. Chem. Soc.* **2005**, *127*, 14172−14173.

(5) Hartwig and co-workers reported the earliest example of σ-CAM for C−H bond functionalization. Several transition metal complexes having metal−boryl σ-bonds showed moderate catalytic activity for borylation of alkanes. Mechanistic studies including DFT calculations suggest that σ-bond metathesis of a metal−boryl σ-bond and a C−H bond seems effective. See: (a) Hartwig, J. F.; Bhandari, S.; Rablen, P. R. *J. Am. Chem. Soc.* **1994**, *116*, 1839−1844. (b) Webster, C. E.; Fan, Y.; Hall, M. B.; Kunz, D.; Hartwig, J. F. *J. Am. Chem. Soc.* **2003**, *125*, 858−859. (c) Hartwig, J. F.; Cook, K. S.; Hapke, M.; Incarvito, C. D.; Fan, Y.; Webster, C. E.; Hall, M. B. *J. Am. Chem. Soc.* **2005**, *127*, 2538−2552.

(6) (a) Langer, R.; Leitus, G.; Ben-David, Y.; Milstein, D. *Angew. Chem., Int. Ed.* **2011**, *50*, 2120−2124. (b) Langer, R.; Diskin-Posner, Y.; Leitus, G.; Shimon, L. J. W.; Ben-David, Y.; Milstein, D. *Angew. Chem., Int. Ed.* **2011**, *50*, 9948−9952. (c) Zell, T.; Milstein, D. *Acc. Chem. Res.* **2015**, *48*, 1979−1994.

(7) (a) Chakraborty, S.; Dai, H.; Bhattacharya, P.; Fairweather, N. T.; Gibson, M. S.; Krause, J. A.; Guan, H. *J. Am. Chem. Soc.* **2014**, *136*, 7869−7872. (b) Fairweather, N. T.; Gibson, M. S.; Guan, H. *Organometallics* **2015**, *34*, 335−339.

(8) (a) Casey, C. P.; Guan, H. *J. Am. Chem. Soc.* **2007**, *129*, 5816−5817. (b) Casey, C. P.; Guan, H. *J. Am. Chem. Soc.* **2009**, *131*, 2499−2507.

(9) (a) Morris, R. H. *Chem. Soc. Rev.* **2009**, *38*, 2282−2291. (b) Sui-Seng, C.; Freutel, F.; Lough, A. J.; Morris, R. H. *Angew. Chem., Int. Ed.* **2008**, *47*, 940−943. (c) Lagaditis, P. O.; Sues, P. E.; Sonnenberg, J. F.; Wan, K. Y.; Lough, A. J.; Morris, R. H. *J. Am. Chem. Soc.* **2014**, *136*, 1367−1380.

(10) (a) Schroeder, M. A.; Wrighton, M. S. *J. Am. Chem. Soc.* **1976**, *98*, 551−558. (b) Frankel, E. N.; Emken, E. A.; Peters, H. M.; Davison, V. L.; Butterfield, R. O. *J. Org. Chem.* **1964**, *29* (11), 3292−3297.

(11) (a) Bart, S. C.; Lobkovsky, E.; Chirik, P. J. *J. Am. Chem. Soc.* **2004**, *126*, 13794−13807. (b) Yu, R. P.; Darmon, J. M.; Hoyt, J. M.; Margulieux, G. W.; Turner, Z. R.; Chirik, P. J. *ACS Catal.* **2012**, *2*, 1760−1764. (c) Chirik, P. J. *Acc. Chem. Res.* **2015**, *48*, 1687−1695. (d) Bart, S. C.; Hawrelak, E. J.; Lobkovsky, E.; Chirik, P. J. *Organometallics* **2005**, *24*, 5518−5527. (e) Hoyt, J.; Shevlin, M.; Margulieux, G. W.; Krska, S. W.; Tudge, M. T.; Chirik, P. J. *Organometallics* **2014**, *33*, 5781−5790.

(12) (a) Daida, E. J.; Peters, J. C. *Inorg. Chem.* **2004**, *43* (23), 7474−7485. (b) Daida and Peters reported oxidative addition of H_2 to a certain Fe(II) phosphine complex and suggested its possible involvement in the catalytic hydrogenation of alkenes. However, no further experimental and theoretical support was provided. See ref 9a.

(13) (a) Chakraborty, S.; Brennessel, W. W.; Jones, W. D. *J. Am. Chem. Soc.* **2014**, *136*, 8564−8567. (b) Chakraborty, S.; Lagaditis, P. O.; Förster, M.; Bielinski, E. A.; Hazari, N.; Holthausen, M. C.; Jones, W. D.; Schneider, S. *ACS Catal.* **2014**, *4*, 3994−4003.

(14) Sunada, Y.; Tsutsumi, H.; Shigeta, K.; Yoshida, R.; Hashimoto, T.; Nagashima, H. *Dalton Trans.* **2013**, *42*, 16687−16692.

(15) For representative ill-defined iron catalysts for hydrogenation of alkenes, see: (a) Harmon, R. E.; Gupta, S. K.; Brown, D. J. *Chem. Rev.* **1973**, *73* (1), 21−52. (b) Rangheard, C.; Fernández, C. J.; Phua, P.-H.; Hoorn, J.; Lefort, L.; de Vries, J. G. *Dalton Trans.* **2010**, *39*, 8464−8471. (c) Manna, K.; Zhang, T.; Carboni, M.; Abney, C. W.; Lin, W. *J. Am. Chem. Soc.* **2014**, *136* (38), 13182−13185.

(16) (a) Prokopchuk, D. E.; Sonnenberg, J. F.; Meyer, N.; Zimmer-De Iuliis, M.; Lough, A. J.; Morris, R. H. *Organometallics* **2012**, *31*, 3056−3064. (b) Lu, X.; Cheng, R.; Turner, N.; Liu, Q.; Zhang, M.; Sun, X. *J. Org. Chem.* **2014**, *79*, 9355−9364. (c) Qu, S.; Dai, H.; Dang, Y.; Song, C.; Wang, Z.-X.; Guan, H. *ACS Catal.* **2014**, *4*, 4377−4388. (d) Langer, R.; Iron, M. A.; Konstantinovski, L.; Diskin-Posner, Y.; Leitus, G.; Ben-David, Y.; Milstein, D. *Chem. - Eur. J.* **2012**, *18*, 7196−7209.

(17) (a) Fong, H.; Moret, M.-E.; Lee, Y.; Peters, J. C. *Organometallics* **2013**, *32*, 3053−3062.

(18) (a) Corey, J. Y. *Chem. Rev.* **2011**, *111*, 863−1071. (b) Corey, J. C.; Braddock-Wilking, J. *Chem. Rev.* **1999**, *99*, 175−292.

(19) (a) Ricci, J. S.; Koetzle, T. F.; Bautista, M. T.; Hofstede, T. M.; Morris, R. H.; Sawyer, J. F. *J. Am. Chem. Soc.* **1989**, *111*, 8823−8827. (b) Van Der Sluys, L. S.; Eckert, J.; Eisenstein, O.; Hall, J. H.;

Huffman, J. C.; Jackson, S. A.; Koetzle, T. F.; Kubas, G. J.; Vergamini, P. J.; Caulton, K. G. *J. Am. Chem. Soc.* **1990**, *112*, 4831−4841. (c) Ho, N. N.; Bau, R.; Mason, S. A. *J. Organomet. Chem.* **2003**, *676*, 85−88. (d) Trovitch, R. J.; Lobkovsky, E.; Chirik, P. J. *Inorg. Chem.* **2006**, *45*, 7252−7260.

(20) (a) Helgaker, T.; Watson, M.; Handy, N. C. *J. Chem. Phys.* **2000**, *113*, 9402−9409. (b) Sychrovsky, V.; Gräfenstein, J.; Cremer, D. *J. Chem. Phys.* **2000**, *113*, 3530−3547. (c) Barone, V.; Peralta, J. E.; Contreras, R. H.; Snyder, J. P. *J. Phys. Chem. A* **2002**, *106*, 5607−5612. (d) Peralta, J. E.; Scuseria, G. E.; Cheeseman, J. R.; Frisch, M. J. *Chem. Phys. Lett.* **2003**, *375*, 452−458. (e) Deng, W.; Cheeseman, J. R.; Frisch, M. J. *J. Chem. Theory Comput.* **2006**, *2*, 1028−1037.

(21) Attempts to search for iron dihydride species by oxidative addition of H_2 to the iron center in **A1** and **B1** failed. The oxidative hydrogen migration from **A1** or **B1** to **A2** or **B2** occurred in a concerted manner. The oxidative addition of H_2 to disilaferracycles ["Fe(II)Si$_2$"] forms "Fe(IV)H$_2$Si$_2$" species via an "Fe(II)(η^2-H$_2$)Si$_2$" intermediate. Calculations of a model compound (see Supporting Information) suggest that the "Fe(IV)H$_2$Si$_2$" species is much less thermodynamically favorable than "Fe(II)(η^2-H$_2$)Si$_2$", suggesting that coordination of ethylene to "Fe(II)Si$_2$" is easy, but oxidative addition of a H−H bond of H_2 on the "Fe(II)Si$_2$" species is difficult.

(22) Recent reviews: Waterman, R. *Organometallics* **2013**, *32* (24), 7249−7263.

(23) Intermediate **A4** has a structure bearing the H−C−C−H "chelate" with two C−H bonds interacting with the metal center, which certainly would not be considered common. However, in silicon chemistry, a similar H−Si−Si−H interaction has been reported by Parken and co-worker, which was obtained by the treatment of Mo(PMe$_3$)$_6$ with H$_2$SiPh$_2$. Zuzek, A. A.; Parkin, G. P. *J. Am. Chem. Soc.* **2014**, *136*, 8177−8180.

(24) As shown in Scheme 3, two energy diagrams of the reaction pathways starting from **A1** and **B1** intersect between **TS$_{A2/A3-\eta^1}$** (**TS$_{B2/B3-\eta^1}$**) and **A3-η^1** (**B3-η^1**). The relative energy of **B1** to **TS$_{B2/B3-\eta^1}$** is higher than that of **A1** to **TS$_{A2/A3-\eta^1}$**, whereas that of **B3-η^1** to **TS$_{B3-\eta^2/A4}$** is lower than that of **A3-η^1** to **TS$_{A3-\eta^2/A4}$**. We calculated possible conversion of **A3-η^1** to **B3-η^1** to produce a new pathway involving all intermediates and transition states with low energy. However, the **A3-η^1** to **B3-η^1** conversion requires >9 kcal/mol, suggesting this new pathway to be less favorable than the original two pathways.

(25) (a) Jessop, P. G.; Morris, R. H. *Coord. Chem. Rev.* **1992**, *121*, 155−284. (b) Kubas, G. J. *Chem. Rev.* **2007**, *107*, 4152−4205.

(26) Balcells, D.; Clot, E.; Eisenstein, O. *Chem. Rev.* **2010**, *110*, 749−823.

(27) There are some reports about the effect of two Si atoms bonded to metal centers. (a) Takagi, N.; Sakaki, S. *J. Am. Chem. Soc.* **2012**, *134*, 11749−11759. (b) Nakatani, N.; Hasegawa, J.; Sunada, Y.; Nagashima, H. *Dalton Trans.* **2015**, *44* (44), 19344−19356.

(28) Smart, K. A.; Grellier, M.; Coppel, Y.; Vendier, L.; Mason, S. A.; Capelli, S. C.; Albinati, A.; Montiel-Palma, V.; Muñoz-Hernandez, M. A.; Sabo-Etienne, S. *Inorg. Chem.* **2014**, *53*, 1156−1165.

(29) One of the reviewers suggested that hydrogenation of a mixture of 1-octene and α-methylstyrene should be performed by catalysis of **1** or Fe(CO)$_5$. The reaction catalyzed by **1** proceeded smoothly to give a mixture of octane and cumene quantitatively. In contrast, slow hydrogenation of 1-octene was observed when Fe(CO)$_5$ was used as catalyst, with α-methylstyrene remaining unreacted. These results clearly support that the catalytically active species generated from **1** is different from that formed from Fe(CO)$_5$.

(30) (a) Kismartoni, L. C.; Weitz, E. *Organometallics* **2005**, *24*, 4714−4720. (b) Wang, W.; Narducci, A. A.; House, P. G.; Weitz, E. *J. Am. Chem. Soc.* **1996**, *118*, 8654−8657.

(31) Asatryan, R.; Ruckenstein, E. *J. Phys. Chem. A* **2013**, *117*, 10912−10932.

(32) Frisch, M. J.; Trucks, G. W.; Schlegel, H. B.; Scuseria, G. E.; Robb, M. A.; Cheeseman, J. R.; Scalmani, G.; Barone, V.; Mennucci, B.; Petersson, G. A.; Nakatsuji, H.; Caricato, M.; Li, X.; Hratchian, H. P.; Izmaylov, A. F.; Bloino, J.; Zheng, G.; Sonnenberg, J. L.; Hada, M.;

Ehara, M.; Toyota, K.; Fukuda, R.; Hasegawa, J.; Ishida, M.; Nakajima, T.; Honda, Y.; Kitao, O.; Nakai, H.; Vreven, T.; Montgomery, J. A., Jr.; Peralta, J. E.; Ogliaro, F.; Bearpark, M.; Heyd, J. J.; Brothers, E.; Kudin, K. N.; Staroverov, V. N.; Keith, T.; Kobayashi, R.; Normand, J.; Raghavachari, K.; Rendell, A.; Burant, J. C.; Iyengar, S. S.; Tomasi, J.; Cossi, M.; Rega, N.; Millam, J. M.; Klene, M.; Knox, J. E.; Cross, J. B.; Bakken, V.; Adamo, C.; Jaramillo, J.; Gomperts, R.; Stratmann, R. E.; Yazyev, O.; Austin, A. J.; Cammi, R.; Pomelli, C.; Ochterski, J. W.; Martin, R. L.; Morokuma, K.; Zakrzewski, V. G.; Voth, G. A.; Salvador, P.; Dannenberg, J. J.; Dapprich, S.; Daniels, A. D.; Farkas, O.; Foresman, J. B.; Ortiz, J. V.; Cioslowski, J.; Fox, D. J. *Gaussian 09*, revision C.01; Gaussian, Inc.: Wallingford, CT, 2010.

(33) Zhao, Y.; Truhlar, D. G. *Theor. Chem. Acc.* **2008**, *120*, 215−241.

(34) Andrae, D.; Häußermann, U.; Dolg, M.; Stoll, H.; Preuß, H. *Theor. Chim. Acta* **1990**, *77*, 123−141.

(35) (a) Gordon, M. S. *Chem. Phys. Lett.* **1980**, *76*, 163−168. (b) Hariharan, Pc; Pople, J. A. *Mol. Phys.* **1974**, *27*, 209−214. (c) Hariharan, Pc; Pople, J. A. *Theor. Chem. Acc.* **1973**, *28*, 213−222. (d) Hehre, W. J.; Ditchfield, R.; Pople, J. A. *J. Chem. Phys.* **1972**, *56*, 2257−2261. (e) Ditchfield, R.; Hehre, W. J.; Pople, J. A. *J. Chem. Phys.* **1971**, *54*, 724−728.

(36) (a) Fukui, K. *J. Phys. Chem.* **1970**, *74*, 4161−4163. (b) Fukui, K. *Acc. Chem. Res.* **1981**, *14*, 363−368. (c) Gonzalez, C.; Schlegel, H. B. *J. Phys. Chem.* **1990**, *94*, 5523−5527.

(37) (a) Krishnan, R.; Binkley, J. S.; Seeger, R.; Pople, J. A. *J. Chem. Phys.* **1980**, *72*, 650−654. (b) McLean, A. D.; Chandler, G. S. *J. Chem. Phys.* **1980**, *72*, 5639−5648. (c) Clark, T.; Chandrasekhar, J.; Spitznagel, G. W.; Schleyer, P. v. R. *J. Comput. Chem.* **1983**, *4*, 294−301.

(38) Miertuš, S.; Scrocco, E.; Tomasi. *Chem. Phys.* **1981**, *55*, 117−129.

(39) Beckmann, J.; Hesse, M. *Z. Anorg. Allg. Chem.* **2007**, *633*, 1233−1238.

(40) (a) Becke, A. D. *Phys. Rev. A: At., Mol., Opt. Phys.* **1988**, *38*, 3098−3100. (b) Becke, A. D. *J. Chem. Phys.* **1993**, *98*, 5648−5652. (c) Lee, C.; Yang, W.; Parr, R. G. *Phys. Rev. B: Condens. Matter Mater. Phys.* **1988**, *37*, 785−789.

(41) (a) Stephens, P. J.; Devlin, F. J.; Chabalowski, C. F.; Frisch, M. J. *J. Phys. Chem.* **1994**, *98*, 11623−11627. (b) Grimme, S. *J. Comput. Chem.* **2006**, *27*, 1787−1799.

(42) (a) B3LYP* functional is a reparametrized version of the B3LYP hybrid functional developed by Reiher and co-workers. Detailed equations are described in the Supporting Information. (b) Reiher, M.; Salomon, O.; Hess, B. A. *Theor. Chem. Acc.* **2001**, *107*, 48−55. (c) Reiher, M. *Inorg. Chem.* **2002**, *41*, 6928−6935. (d) Becke, A. D. *Phys. Rev. A: At., Mol., Opt. Phys.* **1988**, *38*, 3098−3100. (e) Lee, C.; Yang, W.; Parr, R. G. *Phys. Rev. B: Condens. Matter Mater. Phys.* **1988**, *37*, 785−789. (f) Vosko, S. H.; Wilk, L.; Nusair, M. *J. Can. J. Phys.* **1980**, *58*, 1200−1211.

(43) Perdew, J. P.; Wang, Y. *Phys. Rev. B: Condens. Matter Mater. Phys.* **1992**, *45*, 13244−13249.

(44) Grimme, S. *J. Comput. Chem.* **2006**, *27*, 1787−1799.

(45) Throughout the whole discussion in this article, results of calculations performed with the M06 functional were compared with those by B3LYP-D. As summarized in the Supporting Information, geometrical optimization of **1** by B3LYP-D provided structures rather similar to **1a**, **1b**, **1d**, **1e**, and **1f** having two Fe−Si σ-bonds and two "agostic" Si−H groups, as suggested in the previous paper.[14] The bond distances and J_{Si-H} are not very consistent with those determined by crystallography and NMR. Nevertheless, calculated reaction pathways for hydrogenation of ethylene are similar to those of M06, supporting the σ-CAM mechanisms playing important roles on the mechanism.